



Artificial scotoma estimation based on population receptive field mapping

A. Hummer^a, M. Ritter^b, M. Woletz^a, A.A. Ledolter^b, M. Tik^a, S.O. Dumoulin^c, G.E. Holder^{d,e}, U. Schmidt-Erfurth^b, C. Windischberger^{a,*}

^a MR Centre of Excellence, Centre for Medical Physics and Biomedical Engineering, Medical University of Vienna, Währinger Gürtel 18-20, 1090 Vienna, Austria

^b Department of Ophthalmology and Optometry, Medical University of Vienna, Währinger Gürtel 18-20, 1090 Vienna, Austria

^c Spinoza Centre for Neuroimaging, Royal Netherlands Academy of Sciences, Meibergdreef 75, 110BK Amsterdam, Netherlands

^d Department of Ophthalmology, National University of Singapore & National University Hospital, 1E Kent Ridge Road, Singapore 119228, Singapore

^e UCL Institute of Ophthalmology, University College London, 11-43 Bath Street, London EC1V 9EL, UK

ABSTRACT

Population receptive field (pRF) mapping based on functional magnetic resonance imaging (fMRI) is an ideal method for obtaining detailed retinotopic information. One particularly promising application of pRF mapping is the estimation and quantification of visual field effects, for example scotomata in patients suffering from macular dysfunction or degeneration (MD) or hemianopic defects in patients with intracranial dysfunction. However, pRF mapping performance is influenced by a number of factors including spatial and temporal resolution, distribution of dural venous sinuses and patient performance. This study addresses the ability of current pRF methodology to assess the size of simulated scotomata in healthy individuals. The data demonstrate that central scotomata down to a radius of 2.35° (4.7° diameter) visual angle can be reliably estimated in single subjects using high spatial resolution protocols and multi-channel receive array coils.

Introduction

Early lesion studies showed that the topology of an image projected onto the retina is preserved in the visual cortex (Henschen, 1893; Holmes, 1918; Inoue, 1909). Since the late 20th century, functional magnetic resonance imaging (fMRI) has allowed mapping of this retinotopy both in healthy subjects (Serenó et al., 1995) and patients suffering disorders such as macular degeneration (MD) (Baseler et al., 2011; Sunness et al., 2004). Retinotopic maps can be estimated by presenting the subject with phasic stimuli, such as rotating wedges and expanding rings, which periodically stimulate different areas of the retina. The resulting BOLD (blood-oxygen-level dependent) activation of a voxel in the visual cortex can then be correlated to a sinusoid with the stimulus frequency and a specific phase which depends on the voxels corresponding visual field area (Engel et al., 1994). A different method for acquiring retinotopic maps using fMRI is based on population receptive field (pRF) estimates and was introduced by Dumoulin and Wandell in 2008. In the context of retinotopic mapping and fMRI, a receptive field (RF) describes the portion of the visual field, and therefore area of the retina, which has to be stimulated in order to trigger activity in a group of visual cortical neurons. As each visual cortex voxel comprises a vast number of neurons, the visual field leading to an increased BOLD response in a single voxel is referred to as the population receptive field. pRF mapping has been used not only for mapping the visual cortex

in healthy subjects, but also in patient populations with scotomata due to varying ophthalmological causes (Baseler et al., 2011; Papanikolaou et al., 2014).

Different experiments have been conducted using simulated central scotomata in healthy subjects (Baseler et al., 2011; Binda et al., 2013; Haak et al., 2012) to simulate effects of visual system diseases on retinotopic mapping of the visual cortex. Such studies enable the analysis of the effects of locally deprived vision on pRF data and, importantly, allow for arbitrary scotoma layouts and thus establish ground-truth experimental conditions. However, studies in patient populations critically depend on the individual patient's microperimetry performance to approach the “ground-truth” scotoma status and without proper control experiments it is not possible to determine whether changes in retinotopic maps are attributable to plasticity effects in the visual cortex or are merely artefacts of the pRF analysis. For example, Baseler et al. (2011) found that patients with macular degeneration (MD), when compared to healthy controls, show increased pRF sizes in voxels corresponding to the central visual field and a shift of pRF centres towards more peripheral locations and the same effects were also present in healthy controls when stimuli were masked with an artificial scotoma. Besides these analysis-dependent pRF estimate changes, possible feedback from higher visual regions (Williams et al., 2008) and the presence of venous blood in sinuses which reduce sensitivity through magnetic field (B_0) inhomogeneities (Winawer et al., 2010) constitute other

* Corresponding author. Center for Medical Physics and Biomedical Engineering, Medical University of Vienna, Währinger Gürtel 18-20, A-1090 Wien, Austria.
E-mail address: christian.windischberger@meduniwien.ac.at (C. Windischberger).

confounders when investigating small artificial scotomata at the occipital pole.

The present study aims to determine whether it is possible to assess the size of an artificial scotoma using fMRI based on high-resolution multiband-sequence acquisition, despite scotoma-related pRF analysis artefacts, possible extrastriate feedback and B_0 field inhomogeneity effects related to dural sinuses. If successful, accurate scotoma size estimation could allow fMRI-based pRF mapping to become an objective tool for measuring visual field loss independent of patient feedback, thus complementing current approaches such as microperimetry (Papanicolaou et al., 2014) in retinal scotoma patients and enabling or facilitating objective assessment of the effects of potential therapeutic intervention in such patients.

Methods

Subjects

Six healthy subjects (age: 25.8 ± 4.5 years; 3 male, 3 female) were tested. All had normal visual acuity, no history of significant eye disease and gave written informed consent. Subjects were naïve with regard to visual experiments. They were introduced to the stimulus only shortly before the measurement and received no further training. All experiments were approved by the local ethics committee.

MRI measurements

The lower part of a 32-channel head coil (corresponding to a 20 channel head coil itself) was used to examine subjects on a 3T Siemens Tim Trio scanner. BOLD fMRI data of the visual cortex were acquired using the CMRR multiband sequence (Moeller et al., 2010) with TE = 36 ms, TR = 1500 ms, voxel size = $1 \times 1 \times 1 \text{ mm}^3$, 28 slices, multiband factor = 2, distance factor = 10% and 224 vol per run. Slices were aligned orthogonally to the calcarine sulcus and covered 30.8 mm of the occipital cortex. In addition to the functional runs, a structural image was acquired using a magnetization-prepared rapid gradient-echo (MPRAGE) sequence with TE = 4 ms, TR = 2300 ms, voxel size = $1 \times 1 \times 1 \text{ mm}^3$, acquisition matrix = $230 \times 256 \times 160$; field of view = 256 mm.

Stimuli

Moving bar visual stimuli were used, similar to those of Dumoulin and Wandell (2008) as such stimuli are superior to conventional expanding ring stimuli with respect to temporal stability (Senden et al., 2014). Stimuli were generated and controlled in the Matlab programming environment (The MathWorks, Inc., Natick, Massachusetts) using the mrVista software suite (Vista Lab, Stanford University, California).

An 8 Hz flickering checkerboard stimulus, covering the central 18.8° visual angle, was shown to the subjects binocularly. While moving across the screen, a bar with a width of 2.35° visual angle (12.5% of the checkerboard's total width) exposed a section of the flickering checkerboard. Mean luminance was determined by photometric measurement of the luminance of the bright and dark squares of the checkerboard. This mean luminance grey masked the part of the screen not exposed by the bar. As the bar moved slightly after each TR it crossed the screen in 36 s taking 24 discrete steps, each equivalent to 0.78° visual angle. After each crossing of the screen, the bar was rotated by 45° clockwise to cross the screen again in another direction. A grey screen was presented for 12 s after each diagonal crossing. This procedure continued until the bar had travelled in eight different directions across the screen amounting to a total length of 5 min 36 s per run.

There was a central fixation spot with a diameter of 12 pixels (0.22° visual angle) during stimulus presentation. To ensure fixation, subjects were instructed to report colour changes of the spot by pressing a button.

Three modifications of the stimulus, featuring simulated scotomata of different sizes, were presented. These circular scotomata were placed at the centre of the screen and masked the passing stimulus with the grey background colour. The fixation spot remained visible at all times. Artificial scotomata were presented with radii of 1.18° (2.35° diameter), 2.35° (4.7° diameter) and 4.7° (9.4° diameter) visual angle, respectively. Fig. 1 illustrates the different stimulus types. Each run was presented twice, resulting in a total of 8 runs per subject. Run order was randomised across subjects. Due to subject fatigue and technical issues only one full stimulation and one 4.7° scotoma run was recorded for subject 1 and only one 2.35° and one 4.7° scotoma run was recorded for subject 5. Single runs instead of concatenated runs were analysed in these cases.

Analysis

Standard fMRI pre-processing was performed with SPM12 (Wellcome Trust Centre for Neuroimaging, London, UK) and consisted of slice timing correction, realignment and 2 mm FWHM smoothing of functional EPI data. Freesurfer image analysis suite (<http://surfer.nmr.mgh.harvard.edu/>) was used for segmenting MPRAGE datasets of each subject and to create masks of the visual cortical grey matter. Each mask was manually scanned and corrected for topological errors.

For pRF model estimation the two runs of each stimulus type were concatenated. Analysis was carried out using the mrVista toolbox as implemented in Matlab 7.8. First, the pRF of every voxel contained within this mask was modelled as a two-dimensional Gaussian described by parameters x , y for position and σ for size in the visual field. Then, for each voxel the pRF model was combined with the effective stimulus. The time series of the effective stimulus at a certain visual field position was defined as “1” when the stimulus was present, while it was defined as “0” at all other times. The resulting pRF response was convolved with the hemodynamic response function (HRF) which was estimated for each subject to predict the BOLD response of the voxel. The pRF parameters x , y and pRF size (σ) for each voxel were then estimated by minimizing the residual sum of squares between predicted and observed fMRI time series (Dumoulin and Wandell, 2008) by using:

$$RSS = \sum_i (y(t) - p(t)\beta_1)^2 + \beta_2 \quad (1)$$

where $y(t)$ is the data, $p(t)$ are the predictions and β_1 , β_2 are used to scale the predictions for the unknown units of the fMRI signal. While β_1 accounts for the amplitude (slope), β_2 accounts for the intercept. Data were thresholded at 10% explained variance. The analysis was identical for all runs, which means that the pRF estimation algorithm assumed full stimulation of the visual field irrespective of artificial scotoma size. Although it can be advantageous to take the scotoma into account for the analysis in order to obtain accurate pRF parameters (Binda et al., 2013), that option was not used. The primary goal of this study was to estimate scotoma size solely by using fMRI data, which is why providing the analysis software with information about scotoma size would defy the study's purpose. The x and y parameters were converted to polar coordinates (i.e. eccentricity and polar angle) for further analysis.

pRF coverage maps

For subject-specific pRF coverage maps, a two-dimensional Gaussian was centred for each voxel at the visual field position defined by the estimated eccentricity and polar angle parameters. These Gaussian functions had a value of 1 at their centre and their Gaussian spread (standard deviation) is equal to the estimated pRF size of the corresponding voxel. Overlapping Gaussian functions of multiple voxels were combined by using maximum amplitude. This resulted in two-dimensional coverage maps exhibiting values from 0 to 1. The pRF coverage threshold, defining functional visual field areas, was set to 0.5.

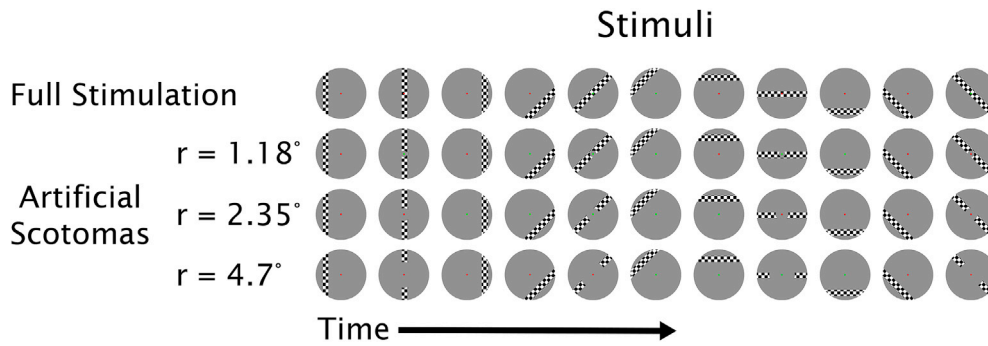


Fig. 1. Illustration of stimuli corresponding to different run types.

Scotoma size estimation

When trying to quantify the size of a scotoma we solely relied on the pRF centre position. In order to compare the size of the scotoma estimated by retinotopic mapping across subjects, histograms were estimated from the eccentricity data, i.e. from the eccentricity values of all supra-threshold V1 voxels. To avoid discretization and an arbitrary choice concerning the number of bins Gaussian Parzen-windows were chosen to create a smooth histogram. This procedure is similar to pRF coverage maps (see above) in the sense that a Gaussian is centred on each pRF centre and the sum of Gaussians is used to create a smooth curve describing pRF centre density. However, in contrast to pRF coverage maps this is a one-dimensional approach in which only eccentricity values are used while the polar angle and pRF size parameter are discarded.

Each histogram was therefore estimated as:

$$H(x) = \frac{1}{\sqrt{2\pi w^2}} \sum_i^N e^{-\frac{(x-r_i)^2}{2w^2}} \quad (2)$$

separately for each subject and run type for all N supra-threshold eccentricity values r_i and width w using Matlab. The appropriate width of the Gaussians was estimated for each subject and run type with the help of Scott's rule (Scott, 1992):

$$w = 3.5 \sigma_r N^{-\frac{1}{3}} \quad (3)$$

This revealed a mean width of $w = 0.4$ which was then chosen for the analysis to make the histograms comparable.

In order to compare pRF centre density relative histograms (rH) were calculated for every subject and scotoma size as:

$$rH = \frac{H_{fullstim} - H_{scotoma}}{H_{fullstim} + H_{scotoma}} \quad (4)$$

where $H_{fullstim}$ corresponds to the concatenated full stimulation runs and $H_{scotoma}$ corresponds to the concatenated runs featuring central scotomata of different sizes. The rH at a certain eccentricity can thus range from +1 to -1:

- $rH = +1$: pRF centres are only present during full stimulation;
- $rH = 0$: no change concerning pRF density when comparing full stimulation and stimulation which is partly concealed by a central scotoma;
- $rH = -1$: pRF centres are only present during stimulation involving a scotoma.

Artificial scotoma sizes can be estimated by using relative histograms that reflect visual stimulation differences with regard to eccentricity. During artificial scotoma runs, only voxels associated with visual field regions more peripheral than the scotoma size should have received stimulus related retinal input. The model should therefore not be able to

explain sufficient variance in scotoma regions, and no pRF centres should be estimated there. The rH is therefore expected to be equal to 1 in these regions. Outside the scotoma region rH should be equal to 0 as the stimulus outside the scotoma does not differ from full stimulation runs.

The possibility of generating relative histograms based on group-averaged full-field stimulation coverage maps was also investigated, as such an approach could be particular useful in patients suffering from retinal scotomata where patient-specific full-field coverage maps are typically unavailable. To this end, 29 full-field stimulation runs of healthy subjects from this study and (Hummer et al., 2016) were averaged to form a mean full-field stimulation histogram. Relative histograms were then calculated based eq. (4) using the group-averaged histogram as $H_{fullstim}$.

Stability

Robustness is an important feature of any visual field testing method. As the reliability of pRF estimates (e.g., eccentricity, polar angle and pRF size) has been previously demonstrated (Senden et al., 2014; van Dijk et al., 2016), the assessment of the stability of the full scotoma size estimation procedure was based on pRF mapping. The stability of quantitative scotoma estimation was investigated by calculating and comparing the relative histograms (see eq. (4)) separately for the first and second simulated scotoma run. The concatenated full stimulation run served as $H_{fullstim}$ for both runs. Separate relative histograms were calculated for all scotoma sizes and subjects. Consistency between first and second run results was then quantified by comparing estimated scotoma sizes based on relative histograms and averaging results over subjects.

Results

The pRF analysis of all full stimulation runs yielded the expected patterns for eccentricity, polar angle and pRF size parameters (Dumoulin and Wandell, 2008). Parameter maps were continuous in the sense that neighbouring voxels corresponded to neighbouring visual field regions. Eccentricity of voxels located at the occipital pole were associated with foveal visual field regions. When examining more anterior visual cortex regions, the voxels eccentricity parameter also increased and represented more peripheral visual field positions. The polar angle for the right visual cortex is close to 180° in the calcarine sulcus, corresponding to the horizontal meridian. For more ventral/dorsal visual cortex regions it decreases/increases until it represents the vertical meridian; it phase reverses at the V1/V2 border. V2d is characterized by decreasing polar angle values up to the horizontal meridian at 180° where the V2d/V3d border is located. In V3d the parameter increases again to the vertical meridian at 270°. Similarly, V2v is characterised by increasing polar angle values to the horizontal meridian at 180° where the V2v/V3v border is located. In V3v the parameter decreases again to the vertical meridian at 90°. Polar angle results of the left visual cortex are mirrored horizontally. The pRF size parameter rises proportional to eccentricity as

voxels associated with foveal regions cover a relatively small visual field region while anterior voxels corresponding to peripheral regions cover larger visual field regions. Fig. 2 shows the pRF parameter maps of a full stimulation run overlaid on the right visual cortex of a typical subject and correlation of eccentricity and pRF size parameters.

pRF coverage maps

Fig. 3 displays eccentricity maps and visual field coverage results of the right primary visual cortex in a single subject. Primary visual cortex V1 is outlined in black and was segmented using the subject's full stimulation polar angle map. In contrast to further analysis, a low variance-explained threshold (1%) was used for segmentation to better illustrate the shape of the visual cortex region. Full stimulation results are shown in the left column. The remaining columns correspond to results from artificial scotomata with radii of 1.18°, 2.35° and 4.7°, respectively.

In the first row, it is clear that increasing scotoma sizes are reflected by increasing cortical areas without sufficient model fit (maps were

thresholded at a level of 10% explained variance). Note that eccentricity maps show only colours corresponding to those visual angles that were actually stimulated, despite the unrestricted and unbiased analysis approach.

The middle row shows the corresponding colour coding, and sizes of the artificial scotomata are depicted by dashed black circles.

The last row of Fig. 3 illustrates the pRF coverage as calculated from fMRI data. In this graph, each dot represents the centre of the receptive field of a single voxel, defined by the eccentricity and polar angle parameter. Every pRF centre is associated with a circular 2D Gaussian centred on the pRF centre with a maximum height of 1 and standard deviation equal to the corresponding pRF size. Gaussians of multiple voxels were combined based on their maximum and together they constitute the pRF coverage map. The pRF coverage range was left at the default value of 0.5–1 i.e. an area of the visual field was classified as functional if the maximum profile of the Gaussian functions was at least 0.5. Dark regions represent a lack of visual stimulation and can be interpreted as a scotoma.

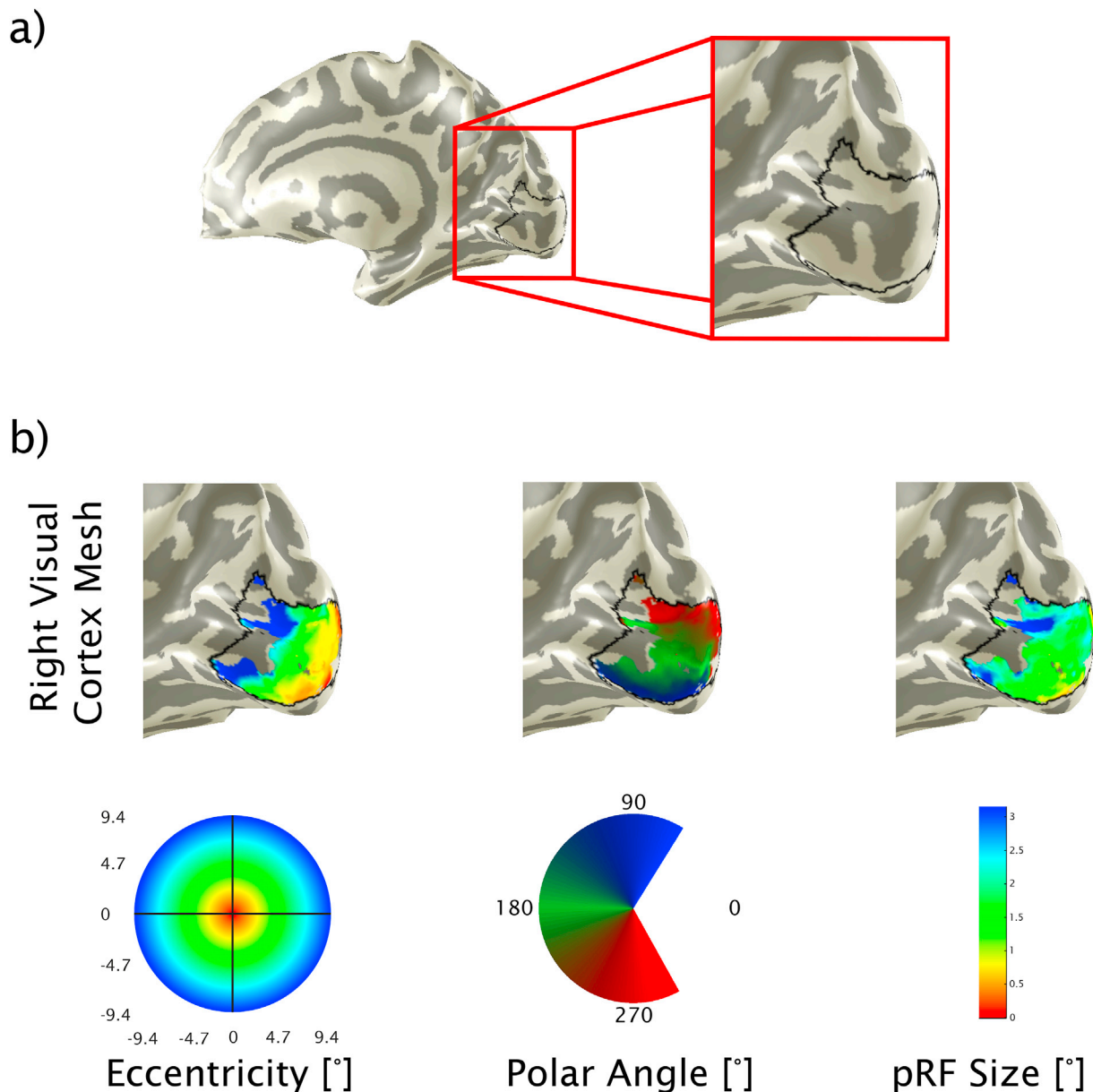


Fig. 2. Subfigure a) highlights the part of the visual cortex mesh enlarged in b), which shows the eccentricity, polar angle, and pRF size parameter for a typical subject's right visual cortex and a regular, full stimulation, run.

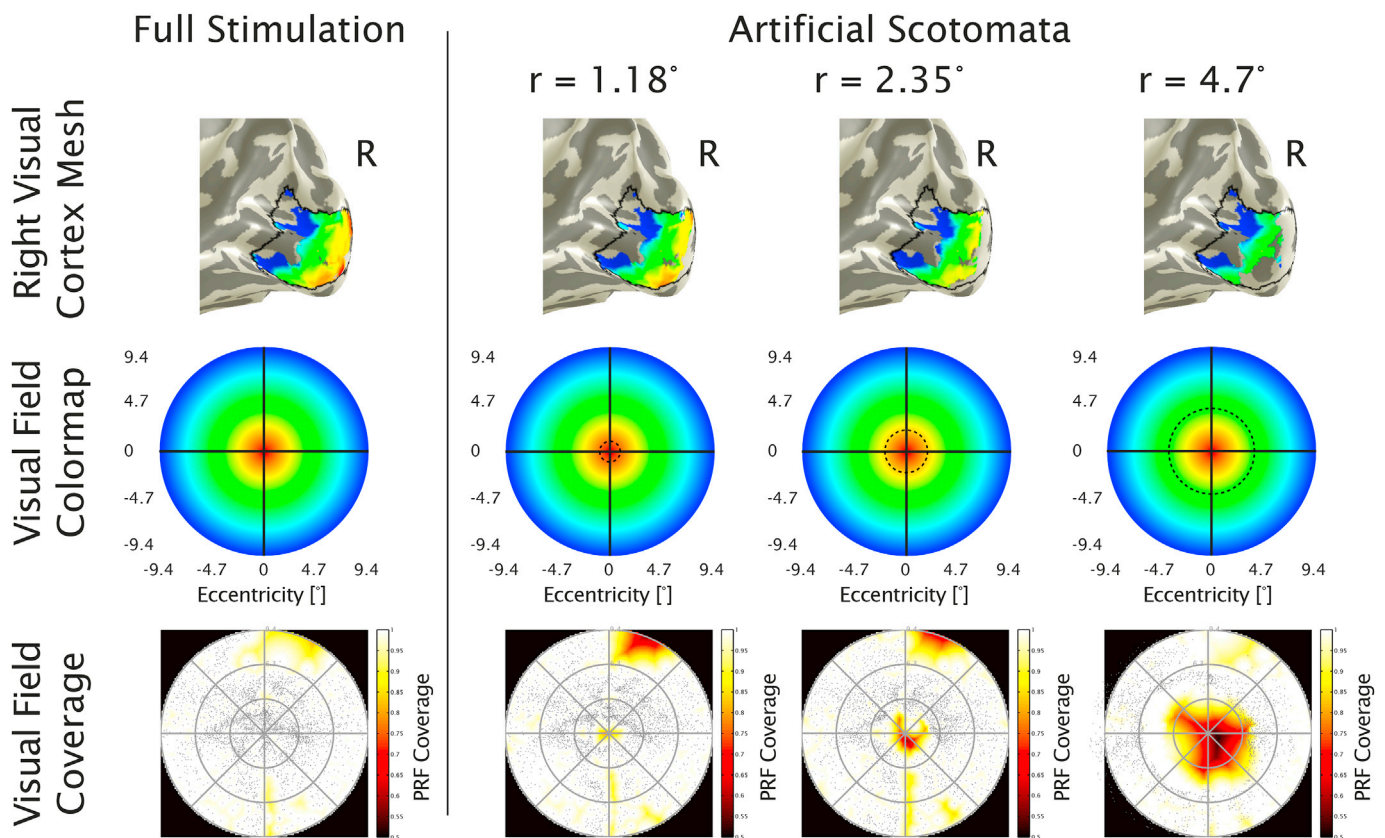


Fig. 3. The first image shows an eccentricity map (>10% variance explained) of the right primary visual cortex of a typical subject. V1 is outlined in black and was segmented using the polar angle map of the subject thresholded at 1% explained variance. The remaining first row images show the eccentricity maps of the same subject corresponding to stimuli involving artificial scotomata of different sizes. The second row shows the corresponding colour circles and, if applicable, the size of the artificial scotomata. The third row illustrates the pRF coverage based on fMRI data. Each dot represents the centre of the receptive field of a single voxel and every pRF centre is associated with a 2D Gaussian (pRF size) which together constitute the coverage map. Dark regions represent a lack of estimated pRFs in this region and therefore a scotoma.

Scotoma size estimation

pRF centre histograms

Histograms of the number of pRF centres over eccentricity values for all supra-threshold (explained variance > 10%) V1 voxels are shown in Fig. 4. The four subplots depict results for full stimulation (left) and all simulated scotoma runs for all subjects. Thin lines represent individual subject results, group-averaged results are plotted with bold blue lines.

Relative histograms

Relative histograms for V1 results and a variance-explained threshold of 10% are shown for each subject and run type in Fig. 5. Mean relative histograms of all subjects are shown in bold blue lines. The curves quite accurately follow the sizes of simulated scotomata. Scotoma sizes were quantified using a threshold of 0.1, yielding sizes estimations of $1.22^\circ \pm 0.50^\circ$ for the 1.18° scotoma, $2.54^\circ \pm 0.18^\circ$ for the 2.35° scotoma and $4.73^\circ \pm 0.27^\circ$ for the 4.7° scotoma (mean \pm standard deviation).

In addition, relative histograms were also calculated for visual cortex regions V2 and V3. A comparison of the group-averaged histograms of V1, V2 and V3 is shown in Fig. 6. Detailed results for V2 and V3 are presented in Supplementary Figs. S1 and S2. In order to examine whether the choice of pRF analysis parameters may be a potential bias in scotoma size estimation, all analyses were repeated using different variance-explained thresholds. Changing the variance-explained threshold will alter the number of voxels to be included in the scotoma size estimation procedure. Fig. 7 shows the group-averaged rH results in V1 for variance-explained thresholds of 0.01, 0.05, 0.1 (default value), 0.15, and 0.2, respectively. Results are remarkably stable; marked deviations are only apparent in the 4.7° radius scotoma case with the lowest variance-explained threshold setting (0.01). Corresponding results for V2 and

V3 appear in Supplementary Figs. S3 and S4.

Relative histograms were also calculated using group-averaged full-field stimulation coverage maps as reference. This approach is particularly useful in scotoma patient studies where scotoma-free stimulation is not an option. In this case, 29 full-field stimulation coverage maps acquired in healthy subjects formed the basis for calculating the group-averaged histogram. Fig. 8 shows the final relative histograms in V1 obtained from using the group-averaged histogram instead of the concatenated full stimulation runs of the individual subjects. Relative histograms across V1, V2 and V3 are plotted in Fig. 9. Results from group-averaged reference histograms are remarkably similar to the plots obtained using subject-specific full-field data (Figs. 5 and 6) indicating little inter-subject variance of full-field stimulation maps.

Stability

The robustness of the procedure was assessed by comparing the scotoma sizes estimated from the first and second run separately. In more detail, relative histograms (see Eq. (4)) were calculated for each of the two runs using the concatenated, full-field stimulation result as reference. Estimated scotoma sizes difference between runs was on average 73.4% for the 1.18° radius scotoma, 9.6% for the 2.35° radius scotoma and 1.5% for the 4.7° radius scotoma. In absolute values this means that, on average, scotoma size estimates for both runs differed by 0.87° for the 1.18° scotoma, 0.23° for the 2.35° scotoma and 0.07° for the 4.7° scotoma.

Discussion

This study used pRF mapping to estimate the sizes of artificial scotomata in healthy individuals. The data demonstrate that simulated

PRF Center Histograms

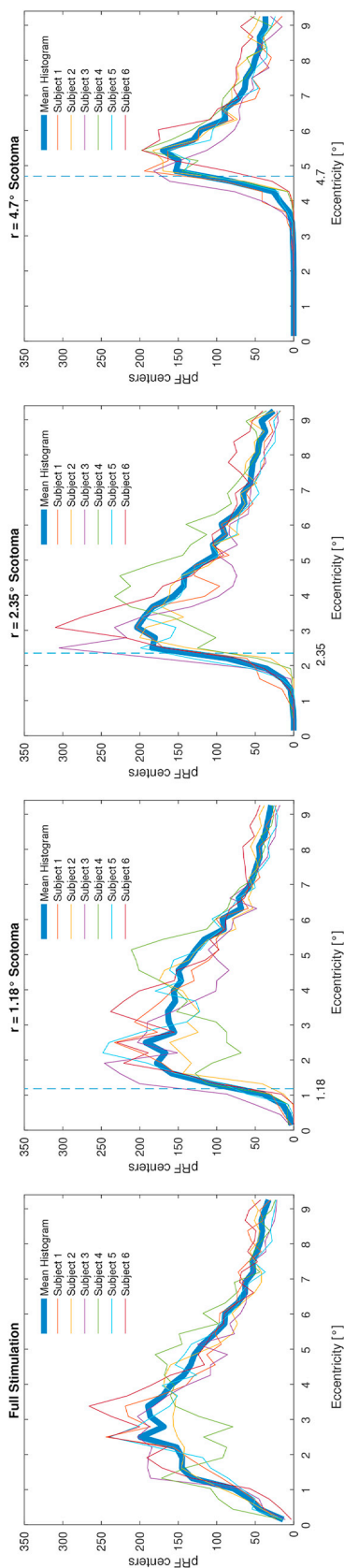


Fig. 4. Line graphs based on pRF center histograms for full stimulation and different simulated scotoma sizes in V1. Radii of presented scotoma are marked with a dashed vertical line. The absolute pRF center count already hints at the artificial scotoma size without the need of a full stimulation run.

scotomata down to a radius of 2.35° (diameter 4.7°) can be accurately estimated in single subjects using pRF analyses using multiband-accelerated high resolution imaging at 3 Tesla.

Comparison to previous studies

Artificial scotomata have been used in several previous studies. Papanikolaou et al. (2014) masked visual field quadrants in healthy subjects for comparison to patients suffering from homonymous field defects. Baseler et al. (2011) investigated MD patients using pRF mapping, but also measured control subjects while presenting them with a stimulus masked by a simulated central scotoma with a radius of 7.5° visual angle. They reported increases of pRF size in voxels associated with the central visual field and pRF centre shifts in MD patients compared to healthy controls. Interestingly, similar effects were also seen when comparing pRF results from artificial scotomata and full-field stimulations in the same healthy controls. Haak et al. (2012) further investigated this effect by scanning healthy subjects and masking the stimulus with two central scotomata of different size (5° and 7.5° visual angle radius). Similarly, they found an increase of pRF size and more peripheral pRF centre locations for voxels associated with the artificial scotoma region. This effect was attributed to the fact that voxel size is in the order of cubic millimetres and the estimated pRFs therefore constitutes an average response of the volume covered. Therefore, pRF estimates will change with partial retinal stimulation as RFs of specific neurons located in the voxel are no longer stimulated. By introducing an artificial central scotoma via restricted visual stimulation, only those RFs will be stimulated which either have sizes sufficient to extent across the border of the scotoma or are smaller in size but more eccentric in location. While this mechanism might explain some of the above findings, feedback from extrastriate areas could also be an important factor as shown in control subjects (Williams et al., 2008) and patients with MD (Masuda et al., 2008) engaged in a stimulus-related task. Binda et al. (2013) also used artificial scotomata (2° visual angle radius) and concluded that the shift of pRF properties can be corrected for by considering the artificial scotomata during pRF estimation. In contrast to the present work, those studies focused on pRF parameter changes due to simulated scotomata and did not attempt to estimate scotoma size, in particular the lower limit of scotoma size resolution. Retinotopy studies dealing with clinical populations suffering from central scotoma (Baker et al., 2005; Baseler et al., 2011; Masuda et al., 2008) were on the other hand mainly concerned with visual cortex plasticity rather than scotoma size estimation.

The acquisition of fMRI data with high spatial resolution is a key factor in the estimation of the size of small scotomata. In this study, improved spatial resolution compared to conventional scans was achieved with the help of the CMRR multiband sequences (Moeller et al., 2010), which enabled the recording of functional imaging data with a resolution of 1 mm³ while maintaining a repetition time of 1.5s. The use of multiband acquisition approaches seems to be a decisive factor for successful scotoma mapping as high-resolution functional imaging significantly reduces partial volume effects and improves retinotopic maps, particularly near the occipital pole (Schira et al., 2009). Due to improved MRI sequences, it was possible to record a multitude of high-resolution scans (an anatomical scan and eight functional scans), simulate different scotoma sizes and perform two runs per stimulus type yet still restrict the measurements to a single session.

Scotoma size estimation using pRF mapping

In this study, polar angle parameters were irrelevant as circular scotomata were assumed, which follows the scotoma shapes often encountered in retinal diseases like macular degeneration (MD) or ABCA4 retinopathy (Stargardt disease). Thus, only the eccentricity parameters were used to estimate scotoma sizes; pRF size was also not taken into consideration. In order to create pRF coverage maps which use the

Scotoma Size Estimation (V1)

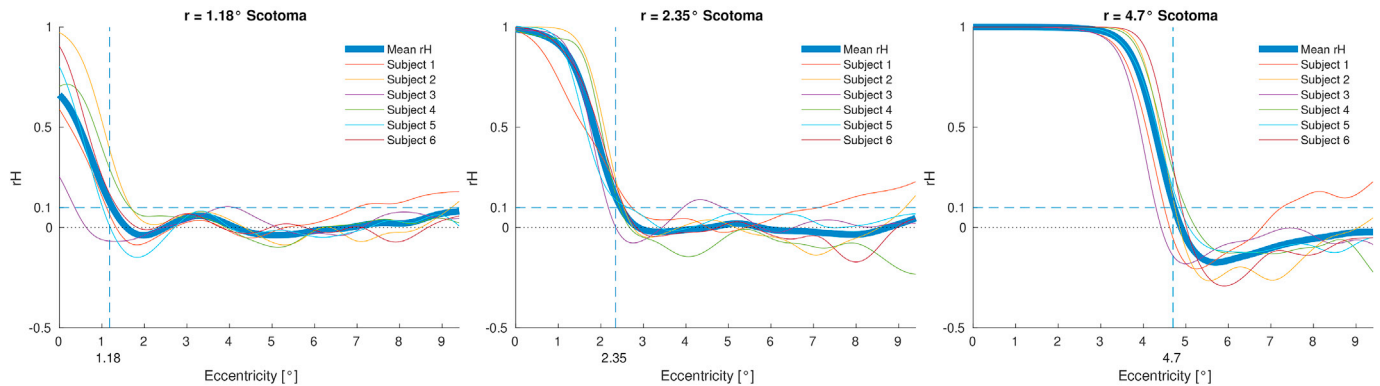


Fig. 5. Relation of pRF centre frequency in full stimulation versus runs containing an artificial scotoma with sizes 1.18°, 2.35° and 4.7° visual angle radius in V1 shown by relative histograms. Data were thresholded with 10% variance explained. The number of estimated pRF centres is strongly reduced inside the simulated scotomata and scotoma size can be estimated fairly accurately at the fall of the curve, especially when examining the mean rHs in thick blue. Radii of presented scotoma are marked with a dashed vertical line, while a rH value of 0.1, which was chosen to quantify scotoma size, is marked with a dashed horizontal line.

Mean rH for different visual cortex regions

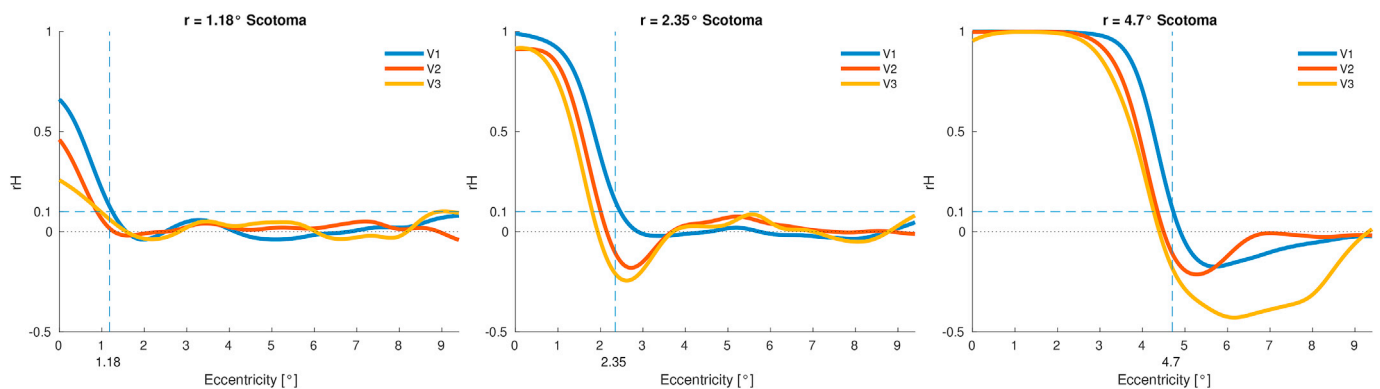


Fig. 6. Mean relative histograms for artificial scotomata of different sizes and visual cortex regions V1, V2 and V3. Data were thresholded with 10% variance explained. Although not as precisely as in V1, scotoma size can be estimated fairly accurate in data originating from voxels located in V2 and V3.

Mean rH for different explained variance thresholds (V1)

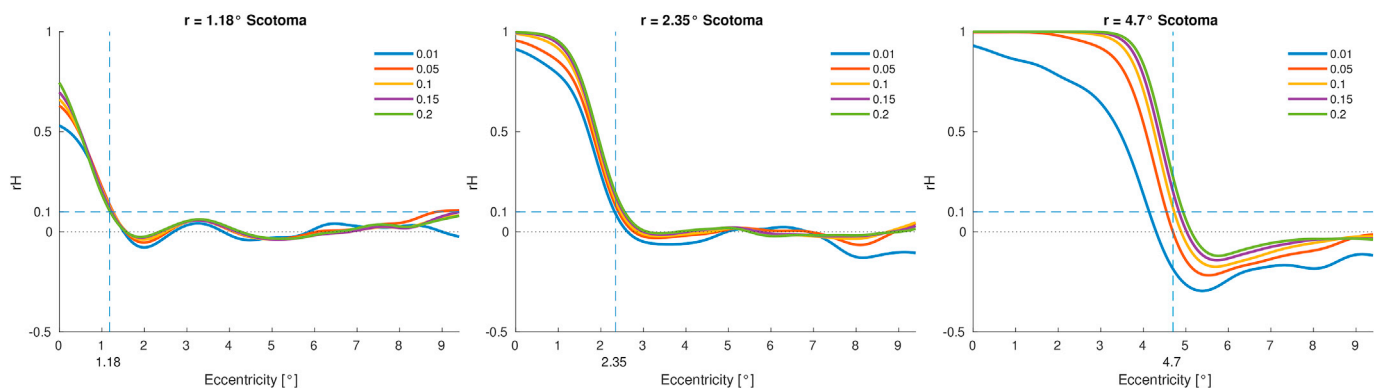


Fig. 7. Mean relative histograms for artificial scotomata of different sizes and various explained variance thresholds for voxels located in the primary visual cortex V1. Lower thresholds show an increased number of estimated pRF centres inside the simulated scotoma which is indicated by lower rH values. An explained variance threshold of 10% was chosen to quantify scotomata as rH curves seem to stabilize above this value.

pRF sizes, it is necessary to define the type of pRF coverage combination method, e.g. how to combine overlapping Gaussians centred at different visual field positions, and the pRF coverage threshold which labels sub-threshold areas as scotoma in order to classify a scotoma based on 2D pRF coverage. Both decisions are rather arbitrary. Additionally, it has been

shown that pRF position estimates are considerably more reliable compared to the pRF size parameter (van Dijk et al., 2016). Analysis herein was therefore limited to the eccentricity parameter of pRF centres. Although the pRF size parameter was omitted, it remained necessary to choose a threshold concerning explained variance determining the voxels

Scotoma Size Estimation (V1)

29 run reference

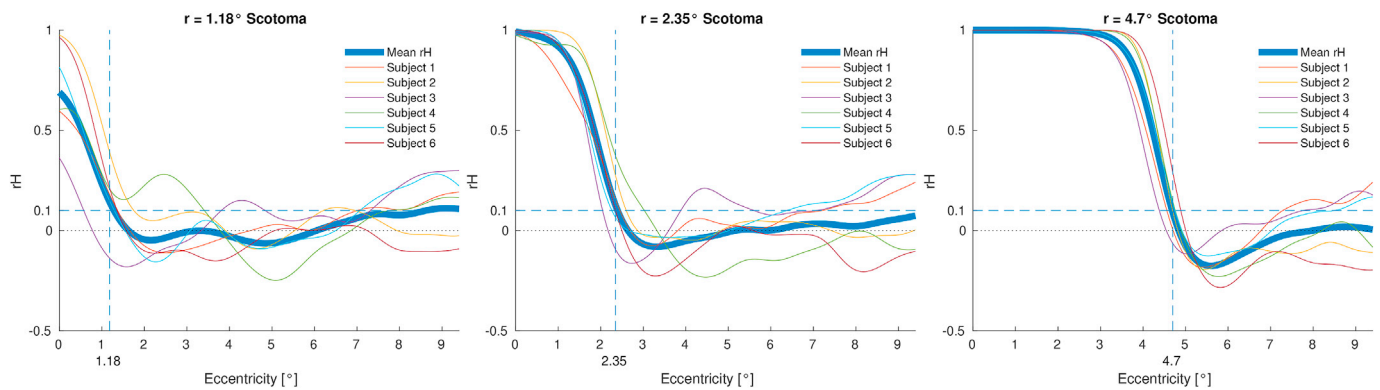


Fig. 8. Relative histograms are shown for different simulated scotoma sizes and voxels located in V1 (explained variance threshold = 10%). In contrast to Fig. 5 rHs are created using a mean histogram of 29 full field runs as reference. Similar to rHs created with individual histogram references these curves allow fairly accurate estimation of scotoma sizes.

Mean rH for different visual cortex regions

29 run reference

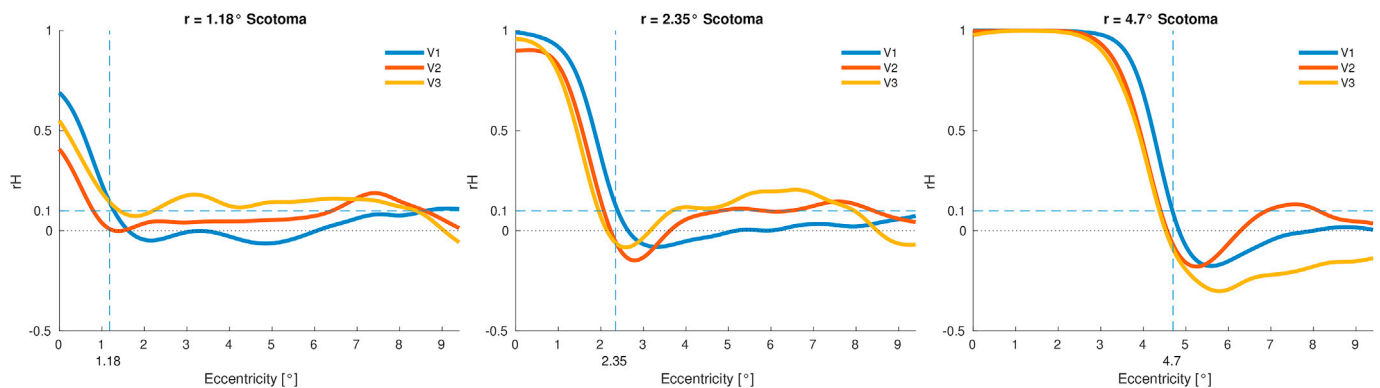


Fig. 9. Mean relative histograms for artificial scotomata of different sizes and visual cortex regions V1, V2 and V3 (explained variance threshold = 10%). In contrast to Fig. 6 rHs are created using a mean histogram of 29 full field runs as reference.

used for each analysis. The chosen threshold of 10% represents a balance between the number of voxels included in the analysis and the reliability of the estimated models associated with these voxels. This is apparent in Fig. 7, figs. S3 and S4 where rH values seem to stabilize for threshold values of 5% and above.

PRF centre histograms

As acquisition of full stimulation may not be possible in clinical settings, it is worth noting that scotoma size estimation is also possible using absolute pRF centre histograms (see Fig. 4). While it may be hard to estimate the size of the smallest scotoma ($r = 1.18^\circ$), there is a distinct change in pRF centre frequency at the border between stimulated and non-stimulated visual field areas in the histograms associated with larger scotomata. For the $r = 2.35^\circ$ and $r = 4.7^\circ$ scotoma it seems realistic to infer the size of the scotoma for each individual subject based on these graphs.

Relative histograms

Despite the different factors affecting artificial scotoma scans including pRF parameter shifts (Haak et al., 2012), dural venous sinuses (Winawer et al., 2010), extrastriate feedback (Williams et al., 2008), partial volume effects (Schira et al., 2009) and microsaccades, the

present data clearly demonstrate accurate estimation and quantification of small scotomata down to a size of 2.35° visual angle radius (4.7° diameter) in single subjects using relative histograms (see Fig. 5). Furthermore, data were acquired in just two five-minute runs for each condition. Although scotoma size cannot be estimated as precisely in V2 and V3, rH curves still show high similarity to the curve based on V1 voxels (see Fig. 6).

Concerning scotoma size estimation, relative histograms also help to reduce false positives. These issues arise most frequently in peripheral regions of the visual field and are related to the general pRF center sparseness in these areas. As full stimulation runs also suffer from this issue a relative measure helps to counteract this problem.

That very small scotoma can be detected (at least in some subjects) by pRF mapping should be taken into consideration when designing tasks covering the centre of the visual field during retinotopic mapping (e.g. a memory game (Binda et al., 2013)), as pRF maps could already be affected.

Individual versus mean histogram reference

An alternative approach to using absolute pRF centre histograms (see above) to estimate scotoma size independent of individual full stimulation runs is to change the reference histogram when calculating relative histograms. Instead of using full stimulation runs of the corresponding

subject it is possible to calculate an average histogram of full-field stimulation runs across multiple sessions and subjects. This makes it possible to relate retinotopic data from patients suffering from scotomata to full-field stimulation runs, which otherwise would not be possible as coverage maps recorded before disease onset are typically not available. In the present study, 29 full stimulation runs of healthy subjects formed the mean full stimulation histogram. This approach seems promising, as relative histograms created with the use of the mean histogram reference are similar to individual reference relative histograms.

Stability

Scotoma estimation stability increases with artificial scotoma size. Although the smallest artificial scotomata with size of 1.18° radius were estimated accurately when considering group-averaged results, single run estimates varied considerably. For scotomata with sizes 2.35° radius (4.7° diameter) and up, intra-subject variations were below 10%. For the largest artificial scotomata examined in this study (4.7° radius, 9.4° diameter), size estimations between runs varied by just 1.5%. The instability in scotoma estimation observed for small scotomata relates to the general challenges encountered in pRF mapping near the occipital pole, most importantly partial volume effects (Schira et al., 2009) and B_0 field inhomogeneity effects related to dural sinuses (Winawer et al., 2010). Possible improvements would be to increase the number of runs, moving to higher field strengths or the use of a custom coil in order to obtain improved SNR. Improving stimulation time of central relative to peripheral regions could also help to enhance data quality and therefore scotoma estimation stability.

Limitations and suggestions for further research

Conventional flickering checkerboard tasks presented as full-field stimuli have been used since the beginning of fMRI (Kwong et al., 1992), and it might be argued that such a technique should enable the estimation of the size of a scotoma. However, even though the presence of a scotoma might be observed in visual cortex data, it cannot be quantified with respect to the corresponding visual field position without prior knowledge. One possibility is first to record a retinotopic map and then perform full-field flickering checkerboard tasks with and without a simulated scotoma (Hoffart et al., 2009). Changes in visual cortex BOLD activation in these trials can then be associated with visual field positions due to the retinotopic map previously recorded. Another method is to stimulate only the artificial scotoma area beforehand to localise the corresponding area on the visual cortex in healthy subjects (Weil et al., 2008). This approach is not possible in case of patients in whom the scotoma layout is unknown. Estimating simulated scotomata using pRF mapping, or retinotopic mapping in general, provides the opportunity simultaneously to investigate the effects of scotomata on visual cortex activation and to link these effects to visual field positions.

The present study was limited to the estimation of central circular scotomata. In contrast to such central scotomata, where minimal size is primarily limited by fMRI measurement parameters (e.g. resolution), estimation of peripheral scotomata will be limited by increased pRF size and reduced cortical magnification factor (Harvey and Dumoulin, 2011). A single voxel with model fit results below threshold can therefore lead to erroneous peripheral dropouts in coverage maps. This is present in the visual field coverage maps of Fig. 3. Density of pRF centres at the top is sparse and pRFs exhibit large pRF size. Conversely, small eccentric scotomata could be masked by adjacent pRFs due to the same effect. Thus, further research should address the correlation between eccentricity and the size of the smallest scotoma that can be reliably estimated. When extending this study to the peripheral visual field, enhancing both the sensitivity and specificity of the pRF method is of importance; this could be achieved by, e.g., increasing the number of runs, enhancing grey/white matter segmentation or improving sensitivity by conducting the study at ultra-high fields (7T and above). Optimization of stimulus

presentation by using eyetracker-based gaze correction as previously reported (Hummer et al., 2016) as well as novel approaches for pRF analysis based on Bayesian inference (Quax et al., 2016; Zeidman et al., 2017) could also lead to improvements.

Another pertinent issue is the occurrence of “filling in” which occurs in some patients with central scotoma (Cohen et al., 2003; Wittich et al., 2006; Zur and Ullman, 2003). It has yet to be determined if the size of the scotoma can be quantified as easily in those patients as in subjects who do not report any such effect.

The presented method is not able to estimate scotoma caused by higher visual area lesions. Patients could suffer a field defect if dysfunction is present in a region receiving feed-forward connections from V1, but a lesion would not be visible in V1. However, striate cortex is particularly suited for pRF mapping, because it is the main receiving area of LGN fibers and concerned with early visual processing (Wandell, 1995).

In clinical context, the data presented herein may help develop predictions regarding fMRI measurements performed in patients after microperimetry, as it should be possible to estimate even small scotomata in fMRI measurements. Furthermore, it would be interesting to monitor scotoma growth in longitudinal studies dealing with patients suffering from macular dysfunction. fMRI estimation of scotoma size could also complement the results of microperimetry (Papanikolaou et al., 2014) in some patients as retinotopy data are less dependent on patients' cooperation/feedback; the only task for the patient is to maintain steady gaze fixation, which can be assisted by displaying a thin cross or a fixation spot at the individual retinal locus. For patients less able to maintain stable fixation on a target it would be possible to use a method where retinotopy data are corrected using concurrently recorded eyetracking data (Hummer et al., 2016).

Conclusion

The results of this study demonstrate that pRF mapping enables size estimation of scotomata down to a radius of 2.35° (4.7° diameter) in single subjects and down to 1.18° (2.35° diameter) in averaged group data. Eccentricity maps obtained from pRF analysis closely match the presented stimulus configuration, suggesting that this method may be applicable for estimating the sizes of small central scotomata in patients, thereby complementing standard microperimetry examination.

Acknowledgements

The authors declare that this work was partially funded by an investigator-initiated and unrestricted research grant from Novartis(CRFB002AAT06T) C. Windischberger acknowledges financial support from the Austrian Ministry of Science, Research and Economy (HSRM project LE103HSK02). G. Holder acknowledges support from NIHR (National Institute for Health Research, UK) and the Foundation Fighting Blindness (USA).

Appendix A. Supplementary data

Supplementary data related to this article can be found at <https://doi.org/10.1016/j.neuroimage.2017.12.010>.

References

- Baker, C.I., Peli, E., Knouf, N., Kanwisher, N.G., 2005. Reorganization of visual processing in macular degeneration. *J. Neurosci. : Offic. J. Soc. Neurosci.* 25, 614–618.
- Baseler, H.A., Gouws, A., Haak, K.V., Racey, C., Crossland, M.D., Tufail, A., Rubin, G.S., Cornelissen, F.W., Morland, A.B., 2011. Large-scale remapping of visual cortex is absent in adult humans with macular degeneration. *Nat. Neurosci.* 14, 649–655.
- Binda, P., Thomas, J.M., Boynton, G.M., Fine, I., 2013. Minimizing biases in estimating the reorganization of human visual areas with BOLD retinotopic mapping. *J. Vis.* 13, 13–13.
- Cohen, S.Y., Lamarque, F., Saucet, J.C., Provent, P., Langram, C., LeGargasson, J.F., 2003. Filling-in phenomenon in patients with age-related macular degeneration: differences

- regarding uni- or bilaterality of central scotoma. *Graefes Arch. Clin. Exp. Ophthalmol.* 241, 785–791.
- Dumoulin, S.O., Wandell, B.A., 2008. Population receptive field estimates in human visual cortex. *Neuroimage* 39, 647–660.
- Engel, S.A., Rumelhart, D.E., Wandell, B.A., Lee, A.T., Glover, G.H., Chichilnisky, E.J., Shadlen, M.N., 1994. fMRI of human visual cortex. *Nature* 369, 525–525.
- Haak, K.V., Cornelissen, F.W., Morland, A.B., 2012. Population receptive field dynamics in human visual cortex. *PLoS One* 7 e37686–e37686.
- Harvey, B.M., Dumoulin, S.O., 2011. The relationship between cortical magnification factor and population receptive field size in human visual cortex: constancies in cortical architecture. *J. Neurosci.* 31, 13604–13612.
- Henschen, S.E., 1893. On the Visual Path and Centre.
- Hoffart, L., Conrath, J., Matonti, F., Wotawa, N., Chavane, F., Ridings, B., Masson, G.S., 2009. A 3T fMRI study of cortical projection of visual scotomas: preliminary results. *J. Fr. Ophtalmol.* 32, 41–49.
- Holmes, G., 1918. Disturbances of visual orientation. *Br. J. Ophthalmol.* 2, 449–468.
- Hummer, A., Ritter, M., Tik, M., Ledolter, A.A., Woletz, M., Holder, G.E., Dumoulin, S.O., Schmidt-Erfurth, U., Windischberger, C., 2016. Eyetracker-based gaze correction for robust mapping of population receptive fields. *Neuroimage* 142, 211–224.
- Inoue, T., 1909. Die Sehstörungen bei Schussverletzungen der kortikalen Sehsphäre, nach Beobachtungen an Verwundeten der letzten japanischen Kriege. Engelmann, Leipzig.
- Kwong, K.K., Belliveau, J.W., Chesler, D.A., Goldberg, I.E., Weisskoff, R.M., Poncelet, B.P., Kennedy, D.N., Hoppel, B.E., Cohen, M.S., Turner, R., et al., 1992. Dynamic magnetic resonance imaging of human brain activity during primary sensory stimulation. *Proc Natl Acad Sci U S A* 89, 5675–5679.
- Masuda, Y., Dumoulin, S.O., Nakadomari, S., Wandell, B.A., 2008. V1 projection zone signals in human macular degeneration depend on task, not stimulus. *Cerebr. Cortex* 18, 2483–2493.
- Moeller, S., Yacoub, E., Olman, C.A., Auerbach, E., Strupp, J., Harel, N., Ugurbil, K., 2010. Multiband multislice GE-EPI at 7 tesla, with 16-fold acceleration using partial parallel imaging with application to high spatial and temporal whole-brain fMRI. *Magn. Reson. Med.* 63, 1144–1153.
- Papanikolaou, A., Keliris, G.A., Papageorgiou, T.D., Shao, Y., Krapp, E., Papageorgiou, E., Stingl, K., Bruckmann, A., Schiefer, U., Logothetis, N.K., Smirnakis, S.M., 2014. Population receptive field analysis of the primary visual cortex complements perimetry in patients with homonymous visual field defects. *Proc Natl Acad Sci U S A* 111, E1656–E1665.
- Quax, S.C., van Koppen, T.C., Jylänki, P., Dumoulin, S.O., van Gerven, M.A.J., 2016. Slice-sampled bayesian PRF mapping. *bioRxiv*.
- Schira, M.M., Tyler, C.W., Breakspear, M., Spehar, B., 2009. The foveal confluence in human visual cortex. *J. Neurosci.* 29, 9050–9058.
- Scott, D.W., 1992. *Multivariate Density Estimation: Theory, Practice, and Visualization*. John Wiley & Sons.
- Senden, M., Reithler, J., Gijzen, S., Goebel, R., 2014. Evaluating population receptive field estimation frameworks in terms of robustness and reproducibility. *PLoS One* 9, e114054.
- Sereno, M.I., Dale, A.M., Reppas, J.B., Kwong, K.K., Belliveau, J.W., Brady, T.J., Rosen, B.R., Tootell, R.B., 1995. Borders of multiple visual areas in humans revealed by functional magnetic resonance imaging. *Science* 268, 889–893.
- Sunness, J.S., Liu, T., Yantis, S., 2004. Retinotopic mapping of the visual cortex using functional magnetic resonance imaging in a patient with central scotomas from atrophic macular degeneration. *Ophthalmology* 111, 1595–1598.
- van Dijk, J.A., de Haas, B., Moutsiana, C., Schwarzkopf, D.S., 2016. Intersession reliability of population receptive field estimates. *Neuroimage* 143, 293–303.
- Wandell, B.A., 1995. *Foundations of Vision*. Sinauer Associates, Inc.
- Weil, R.S., Watkins, S., Rees, G., 2008. Neural correlates of perceptual completion of an artificial scotoma in human visual cortex measured using functional MRI. *Neuroimage* 42, 1519–1528.
- Williams, M.A., Baker, C.I., Op de Beeck, H.P., Shim, W.M., Dang, S., Triantafyllou, C., Kanwisher, N., 2008. Feedback of visual object information to foveal retinotopic cortex. *Nat. Neurosci.* 11, 1439–1445.
- Winawer, J., Horiguchi, H., Sayres, R.A., Amano, K., Wandell, B.A., 2010. Mapping hV4 and ventral occipital cortex: the venous eclipse. *J. Vis.* 10, 1.
- Wittich, W., Overbury, O., Kapusta, M.A., Watanabe, D.H., Faubert, J., 2006. Macular hole: perceptual filling-in across central scotomas. *Vis. Res.* 46, 4064–4070.
- Zeidman, P., Silson, E.H., Schwarzkopf, D.S., Baker, C.I., Penny, W., 2017. Bayesian population receptive field modelling. *Neuroimage*.
- Zur, D., Ullman, S., 2003. Filling-in of retinal scotomas. *Vis. Res.* 43, 971–982.